HHS Public Access

Author manuscript

J Surg Res. Author manuscript; available in PMC 2021 July 01.

Published in final edited form as:

J Surg Res. 2020 July ; 251: 239–247. doi:10.1016/j.jss.2020.01.028.

SPECT imaging using formyl peptide receptor 1 ligand can diagnose aortic aneurysms in a mouse model

Alexander H. Shannon[a], **Mahendra D. Chordia**[b], **Michael D. Spinosa**[a], **Gang Su**[c], **Zachary Ladd**[c], **Dongfeng Pan**[b], **Gilbert R. Upchurch Jr.**[c], **Ashish K. Sharma**[c]

[a]Department of Surgery, University of Virginia, Charlottesville, VA

[b]Department of Radiology and Medical Imaging, University of Virginia, Charlottesville, VA

[c]Department of Surgery, University of Florida, Gainesville, FL

Abstract

Background: Our previous studies showed that neutrophil infiltration and activation plays an important role in the pathogenesis of abdominal aortic aneurysms (AAA). However, there is a lack of noninvasive, inflammatory cell-specific molecular imaging methods to provide early diagnosis of AAA formation. Formyl peptide receptor 1 (FPR1) is rapidly upregulated on neutrophils during inflammation. Therefore, it is hypothesized that use of cFLFLF, a PEGylated peptide ligand that binds FPR1 on activated neutrophils, would permit accurate and noninvasive diagnosis of AAA via single photon emission computed tomography (SPECT) imaging.

Materials and Methods: Male C57BL/6 (WT) mice were treated with topical elastase (0.4 U/ml type 1 porcine pancreatic elastase) or heat inactivated elastase (control) and aortic diameter was measured by video micrometry. Comparative histology was performed on day 14 to assess neutrophil infiltration in aortic tissue. We performed near-infrared fluorescence imaging using c-FLFLF-Cy7 probe on days 7 and 14 post-elastase treatment and measured fluorescence intensity *ex vivo* in excised aortic tissue. Separate group of animals were injected with ^{99m}Tc-c-FLFLF two hours prior to SPECT imaging on day 14 using a SPECT/CT/PET trimodal scanner. Co-expression of neutrophils with c-FLFLF was also performed on aortic tissue by immunostaining on day 14.

Results: Aortic diameter was significantly increased in the elastase group compared to controls on days 7 and 14. Simultaneously, a marked increase in neutrophil infiltration and elastin degradation, as well as decrease in smooth muscle integrity, was observed in aortic tissue after elastase-treatment compared to controls. Moreover, a significant increase in fluorescence intensity of c-FLFLF-Cy7 imaging probe was also observed in elastase-treated mice on day 7

Corresponding Author: Ashish K. Sharma, MBBS, PhD, Associate Professor, Department of Surgery, University of Florida, Gainesville, FL 32610, ashish.sharma@surgery.ufl.edu, Phone: (352) 294-8660.

Authors' contributions: A.H.S, M.D.C., M.D.S., G.S., Z.L. conducted the experiments. A.H.S., M.D.C., D.P., G.R.U. and A.K.S. contributed to article drafting. G.R.U. and A.K.S. worked on article editing.

Disclosure

All authors declare no conflicts of proprietary or commercial interest.

(approximately 2-fold increase) and day 14 (approximately 2.5-fold increase) compared to respective controls. SPECT imaging demonstrated a multi-fold increase in signal intensity for ^{99m}Tc-cFLFLF radiolabel probe in mice with AAA compared to controls on day 14. Immunostaining of aortic tissue with c-FLFLF-Cy5 demonstrated a marked increase in co-expression with neutrophils in AAA compared to controls.

Conclusions: cFLFLF, a novel FPR1 ligand, enables quantifiable, noninvasive diagnosis and progression of AAAs. Clinical application of this inflammatory cell-specific, molecular probe using SPECT imaging may permit early diagnosis of AAA formation, enabling targeted therapeutic interventions and preventing impending aortic rupture.

Keywords

Vascular imaging; SPECT scans; Formyl peptide receptor; Abdominal aortic aneurysms; Aortic Inflammation

Introduction

Abdominal aortic aneurysm (AAA) is an insidious disease, affecting 7% males older than 65.[1, 2] Development of aneurysms is generally asymptomatic until impending rupture, which is associated with a 50% pre-hospital mortality and accounts for approximately 15,000 deaths annually in the United States.[3] The current standard of patient care in these cases is surveillance with imaging followed by surgery, via open or endovascular intervention, once symptoms such as abdominal pain develop or the aneurysm has grown above 5.5 cm or 5 cm for males and females, respectively.[4, 5] Currently, there are no known medical therapies or pharmaceutical strategies to attenuate AAA formation and prevent impending aortic rupture.

Vascular inflammation and subsequent remodeling has been shown to play a pivotal role in the pathogenesis of AAA.[6, 7] Previous studies from our group and others have implicated polymorphonuclear neutrophils (PMN) infiltration and activation as playing a prominent role in AAA formation.[8–10] However, the ideal imaging modality to quantify, describe, and identify inflammation, including PMN infiltration, within early aortic aneurysms *in vivo*, continues to elude clinical practice which mostly relies on ultrasound-based imaging of aneurysm size. Single-photon emission computed tomography (SPECT) imaging has shown promise as a noninvasive modality to characterize leukocytes' role in the inflammatory cascade in a myriad of pathologic processes via tagging with an imaging probe called cinnamoyl-F-(D)L-F-(D)L-F-K (cFLFLF).[11–15] This probe, when linked with polyethylene glycol (PEG), gives it a favorable pharmacokinetic profile, and targets formyl peptide receptor 1 (FPR1), a G-protein coupled receptor, which is over expressed in activated PMNs.[16, 17] The complex of technetium-99m (^{99m}Tc) to this peptide allows visualization of inflammatory foci with SPECT imaging is plausible wherein activated neutrophils have accumulated under inflammatory conditions.[11] The application of ^{99m}Tc-cFLFLF using SPECT imaging may fill the void of noninvasive imaging techniques required to characterize inflammation, provide early diagnosis of AAA, and predict the risk of impending aortic rupture.

Therefore, the objective of this study was to investigate the diagnostic ability of *in vivo* neutrophil labeling with ^{99m}Tc-cFLFLF using SPECT imaging in a murine model of AAA. We hypothesize that use of c-FLFLF will bind FPR1 receptors on activated PMNs accrued in the inflamed aortic tissue and permit accurate, noninvasive diagnosis of AAA via SPECT imaging.

Materials and Methods

Elastase treatment model of AAA

C57BL/6 wild-type male mice (8- to 12-weeks old, The Jackson Laboratory, Bar Harbor, ME) were anesthetized using isoflurane and underwent midline laparotomy with evisceration of abdominal contents to expose the infra-renal abdominal aorta. The infra-renal abdominal aorta was dissected away from the surrounding tissues and inferior vena cava and either 5 microliters of porcine pancreatic elastase (0.4 U/ml type 1 porcine pancreatic elastase, Sigma Aldrich, St. Louis, MO, USA) or heat inactivated elastase (deactivated elastase, serving as control) was topically applied to the exposed aorta. Topical elastase remained on the aorta for 5 minutes and then excess was removed with a sponge. The abdominal viscera were returned to the peritoneal cavity and the abdominal wall was closed in layers. Appropriate analgesics were given intraperitoneally for pain relief (0.02 ml Buprenorphine). Mouse aortas were procured on either post-operative day 7 or 14, and preserved in formalin for tissue analysis. Four groups of animals were compared: mice treated with deactivated elastase with aortic procurement at day 7 (Control Day 7) or day 14 (Control Day 14) and mice treated with elastase with aortic procurement at day 7 (Elastase Day 7) or day 14 (Elastase Day 14). Aortic diameter was determined using video photomicrometry using Leica Application Suite 4.3 software (Leica Microsystems, Buffalo Grove, IL, USA). Aortic dilatation (%) was calculated as follows: [(maximal abdominal aortic diameter– internal control abdominal aortic diameter/internal control abdominal aortic diameter) X 100%)]. The animal protocol was approved by the University of Virginia Institutional Animal Care and Use Committee (protocol #3634) in compliance with the Office of Laboratory Animal Welfare.

^{99m}Tc-c-FLFLF SPECT imaging probe

We have previously described the synthesis and validation of cFLFLF as a peptide ligand to FPR1.[11, 14] We have also shown that ^{99m}Tc-cFLFLF is a neutrophil specific radioligand for SPECT imaging.[11, 14] ^{99m}Tc-cFLFLF was synthesized using PEGylated cFLFLF conjugated with hydrazinonicotinamide and complexed with ^{99m}Tc for SPECT imaging. The PEGylated cFLFLF was also labeled with Cy5-NHS or Cy5-NHS esters (Sigma-Aldrich, St. Louis, MO) for *in vivo* and *ex vivo* fluorescence imaging, respectively.

SPECT/CT Imaging

SPECT/CT was performed on the Albira Si Trimodal pre-clinical scanner (Bruker) comprised of PET, SPECT and CT sub-systems. SPECT/CT modalities are coplanar with the SPECT imaging module fitted with two opposing 180-degree gamma cameras. The CT module, X-ray emitter and detector are placed orthogonal to SPECT module. Two separate groups of mice (elastase treated and heat inactivated elastase controls) were injected with

200 μL of ^{99m}Tc-c-FLFLF (40–60 MBq) via tail vein injection two hours prior to imaging on post-operative days 7 and 14. After two hours of tracer injection, the animals were anesthetized using continuous inhaled isoflurane (2–3% in oxygen), the mouse was placed supine in a smallest cassette provided by Albira equipped with controlled temperature and SPECT imaging was performed using 1.0 mm single pinhole collimator (SPH) with 50 mm field of view. The CT module is equipped with variable current and voltage has an axial FOV of 65 mm. Upon completion of SPECT, computed tomography (CT) acquisition was performed using high voltage setup in standard protocol. Automated reconstruction of tomograph was achieved with no attenuation or scatter correction using the ordered subsets expectation-maximization (OSEM) routine provided by Albira Software Suite. Image (cubic) voxel size ranges from 0.28 mm (25 mm FOV) to 1.0 mm (120 mm FOV). The reconstructed SPECT and CT images were processed, fused and analyzed with π.pmode software (3.8 version, PMOD Technologies LLC, Zurich, Switzerland). Organ uptake of ^{99m}Tc-cFLFLF was measured using a gamma counter (Perkin Elmer, Waltham, MA) and reported as a relative percentage of total radioactivity of harvested aortic tissue and normalized to tissue weight, and injected dose to animal body weight.

Near-infrared Fluorescence Imaging

Near-infrared Fluorescence imaging was performed on a separate group of animals by using c-FLFLF-Cy7 probe on day 7 and 14 post-elastase treatment 2 hours prior to imaging. Mice received a tail-vein injection of 100 μL of c-FLFLF-Cy7 probe (2nM), and then after two hours were imaged with IVIS Spectrum Fluorescence Imaging system (excitation 745 nanometers (nm), emission 820 nm; PerkinElmer, Inc., Waltham, MA) for near infrared fluorescence. After imaging, animals were euthanized with subsequent organ and aortic procurement. Fluorescence intensity was measured *ex vivo* using the same Imager. Total fluorescence intensity was obtained for each aneurysm by focusing on a region of interest incorporating the entire aortic sample.

Histology

Murine AAA specimens were harvested and fixed in 10% formalin. After 24 hours, fixed samples were embedded in paraffin, and sections were stained by immunohistochemistry as previously reported.[18] Aortic sections were also stained with hematoxylin and eosin, and Verhoeff-Van Gieson for elastin. For neutrophil immunostaining, the aorta sections (5μm) were dehydrated and incubated with 1% hydrogen peroxide followed by boiling in 1X unmasking solution (Vector Laboratories, Burlingame, CA) for 15 minutes and blocked with 10% serum. After antigen retrieval, antibodies were bound and detected using VectaStain Elite Kit (Vector Laboratories Inc., Burlingame, California). Antibodies for IHC staining were anti-mouse anti-Neutrophil (Ly6B.2) for neutrophils (1:10,000; AbD Serotec, Oxford, United Kingdom). Visualization color development was completed using diaminobenzidine (Dako Corporation, Carpinteria, California) to produce a brown precipitate. Sections were then counterstained with hematoxylin. For smooth muscle α-actin (SM-αA) staining, the alkaline phosphatase-conjugated monoclonal anti–SM-αA antibody (Sigma, St Louis, MO) was used. Images were acquired using 20X magnification by an Olympus microscope equipped with an Olympus digital camera, and ImagePro software. Quantification of histological distribution for each group was performed according to the following grading:

Neutrophil staining: 1 = none to few, 2 = mild, 3 = moderate, 4 = extensive; Smooth muscle alpha actin staining: 1 = none to few, 2 = mild, 3 = moderate, 4 = extensive; Elastin staining: 1= concentric heavy rings of elastin, 2 = mild elastolysis, 3 = moderate elastolysis, 4 = extensive elastolysis.

Immunofluorescence staining of aortic tissue

Co-expression of neutrophils (Ly6G-FITC) and c-FLFLF-Cy5 was performed by immunostaining of aortic tissue on post-operative day 14, using immunofluorescence staining as described previously.[19] Briefly, aortic tissue sections were incubated with anti-mouse Ly6G-FITC antibody (1:100, Biolegend) and c-FLFLF-Cy5 peptide (2nM, 1:100) at 4° C overnight. Images were obtained with an Olympus IX81 inverted confocal microscope (Olympus Corp) with a CCD camera at 200X or 400X magnification. The images were processed using slidebook 6 software (3I Digital microscopy imaging, Denver, CO). For intensity quantification of fluorescence, images were analyzed by ImageJ software (National Institute of Health, Bethesda, MD), measuring the mean intensity of corresponding sections of the respective sections.

Statistical Analysis

Values are presented as the mean ± standard error of mean and statistical evaluation was performed using GraphPad Prism 6 software (GraphPad, La Jolla, CA). One-way analysis of variance (ANOVA) after post-hoc Tukey's test was used to determine the differences among multiple comparative groups. Unpaired t-test with nonparametric Mann-Whitney test was also used for pair-wise comparisons of groups. *P* value less than 0.05 was considered statistically significant.

Results

Neutrophil infiltration is an early event during AAA formation

Using the topical elastase-treatment model of AAA, we observed a significant increase in aortic diameter on days 7 and 14 in WT mice compared to heat-inactivated elastase controls (Fig. 1). Significant increase in aortic diameter was observed in elastase-treated mice on day 7 compared to respective controls (130.1±9.3% vs. 2.2±0.9%; $p<0.0001$; Fig. 1B–C). Similarly, elastase-treated WT mice had the maximum increase in aortic diameter compared to respective controls on day 14 (154±11.9% vs. 4.9±4.2%; $p<0.0001$). Aortic diameter was observed to be the highest on day 14, however it was not significantly different than day 7 (154±11.9% vs. 130.1±9.3%; $p=0.3$). Also, elastase-treated mice demonstrate increased neutrophil infiltration, distorted aortic morphology as seen by decrease in smooth muscle α-actin expression as well as decrease in elastic fiber disruption compared to controls on days 7 and 14 (Fig. 2).

Fluorescence imaging of AAA with Cy7-cFLFLF

We performed near-infrared fluorescence imaging using Cy7-cFLFLF in WT mice on days 7 and 14 after elastase treatment and respective controls. The cFLFLF fluorescence intensity was found to be markedly increased in the elastase-treated groups compared to respective controls both on days 7 and 14 (Fig. 3A–B). *Ex vivo* fluorescence imaging also confirmed

and demonstrated increased Cy7-cFLFLF intensity in elastase-treated aortas compared to controls on day 14 (Fig. 3C). Upon quantification of *ex vivo* aortic tissue, a significant increase in fluorescence intensity of c-FLFLF was observed in elastase-treated mice compared to controls on day 7 ($3.9\times10^{03}\pm0.4\times10^{2}$ vs. $1.9\times10^{03}\pm0.1\times10^{02}$ RFU; relative fluorescence units; p=0.03) and day 14 ($6.3\times10^{03}\pm0.7\times10^{2}$ vs. $2.6\times10^{03}\pm0.2\times10^{02}$ RFU; p=0.0001), respectively (Fig. 3D). A significant increase in c-FLFLF florescence intensity was observed in elastase-treated mice on day 14 compared to day 7 ($6.3\times10^{03}\pm0.7\times10^{2}$ vs. $3.9\times10^{03}\pm0.4\times10^{2}$ RFU; p=0.009).

SPECT/CT imaging of AAA with ^{99m}Tc-cFLFLF

SPECT/CT imaging with ^{99m}Tc-cFLFLF permitted imaging of AAA obtained on day 14. Use of SPECT/CT imaging with the FPR1 ligand (^{99m}Tc-cFLFLF) demonstrated a marked increase in probe uptake at the site of AAA compared to controls (Fig. 4A). Moreover, there was a significant increase in ^{99m}Tc-cFLFLF radioactivity in excised aortic tissue of elastase-treated mice compared to controls (Fig. 4B). Importantly, the ^{99m}Tc-cFLFLF uptake correlated with increase in neutrophil infiltration and aortic diameter phenotype, thereby enhancing the importance of this non-invasive imaging technique in diagnosing aortic inflammation and vascular remodeling during AAA.

cFLFLF labels neutrophils in AAA tissue

Immunofluorescent staining of aortic sections demonstrated that control mice demonstrated few neutrophils and minimal Cy7-cFLFLF expression (Fig. 5A, **top**). However, in the elastase-treated mice there was a marked increase in neutrophil infiltration and more importantly, cFLFLF-Cy5 binding was largely limited to infiltrating neutrophils as demonstrated by increased co-expression of cFLFLF-Cy5 with anti-Ly6G-FITC (Fig. 5A, **bottom**). Quantification of same normalized areas of imaging showed a significant increase in fluorescence intensity of c-FLFLF-Cy5 and Ly6G-FITC (Fig. 5B). This data demonstrates that c-FLFLF can bind neutrophils in aortic tissue to signify the presence of inflammation during AAA formation.

Discussion

This study demonstrates the feasibility of using a novel FPR1 imaging ligand, cFLFLF, to noninvasively identify aortic inflammation in AAAs to help make the diagnosis as well as aiding in the progression of AAAs. In a murine model of AAA formation, mice treated with topical elastase to induce aneurysm formation had a markedly enhanced ^{99m}Tc-cFLFLF signal intensity compared to controls on post-operative day 14 using SPECT scans. Importantly, results of SPECT/CT scans, a clinically relevant imaging modality, correlated with increase in aortic diameter and neutrophil infiltration as well as vascular remodeling observed in AAA tissue compared to controls. Additionally, a significant increase in fluorescence intensity was observed in elastase-treated mice on days 7 and 14 compared to their respective controls using fluorescence imaging. The clinical application of cell-specific, molecular imaging probes such as cFLFLF may permit early diagnosis of AAA as well as track the progression of AAA. This may enable targeted therapeutic interventions to

monitor aortic inflammation, vascular remodeling and AAA progression to prevent impending aortic rupture.

AAAs are an indolent disease process, often asymptomatic until rupture is imminent.[20] Aortic rupture is generally a catastrophic event with an associated mortality ranging from 75–90%.[21] Surveillance with CT scans or ultrasound allows macroscopic evaluation of aortic diameter, which is used as a gauge for when surgical intervention is indicated. However, these modalities fail to assess the complicated underlying pathophysiology of AAA, including the role of inflammation, and more specifically, leukocytes such as PMNs, play in their formation.[8, 22] Molecular imaging modalities have come to the forefront as noninvasive ways to characterize the complexity of AAA pathophysiology and develop potential prognostic indicators and therapeutic interventions. Currently, the gold standard of molecular imaging of inflammation is *ex vivo*, with removal of cells followed by tagging and subsequent re-injection of cells, which is fraught with complication.[23] Molecular imaging modalities *in vivo* have been attempted using monoclonal antibodies with limited success.[23] Novel *in vivo* molecular imaging techniques are currently being investigated, including magnetic resonance imaging (MRI), positron emission tomography (PET), and SPECT, each with its own strengths and weaknesses.

Ultra small super-paramagnetic iron oxide (USPIO)-enhanced magnetic resonance imaging has been utilized to image macrophage infiltration in carotid and aortic atheromas in both animal models and *in vivo* human studies.[24–28] Advantages of molecular MRI include high soft tissue contrast, high spatial and temporal resolution, and avoidance of ionizing radiation and nephropathy associated with contrast administration.[29] However, endogenous iron present from hemorrhage or intramural thrombus found within the aneurysmal wall hinders the utility of this imaging modality for inflammation evaluation.[30] PET/CT scanning has also initially shown promise with the utilization of ^{18}F-fluorodeoxyglucose (^{18}F-FDG), which is correlated with rapid aortic enlargement and rupture.[31] ^{18}F-FDG is a PET contrast agent that binds glucose transporter proteins (GLUT) in a competitive manner with glucose in metabolically active cells, including inflammatory cell. We have previously demonstrated increased ^{18}F-FDG uptake in micro-PET imaging that was associated with increased inflammation in ruptured AAA walls in a rat rupture model, which was also confirmed by another study by Courtois *et al.* [32, 33] ^{18}F-FDG metabolism and uptake does relate to leukocyte infiltration in blood vessel walls, however it is a non-specific marker for inflammation, with uptake proportional to metabolic activity of the cell.[34] All metabolically active cells absorb ^{18}F-FDG and therefore, due to this lack of specificity in determining cell types associated with inflammatory processes, does not appear to be the ideal modality for assessing progression of inflammation in AAA.

SPECT imaging has been introduced as an alternative non-invasive method to more specifically identify pro-inflammatory PMNs within the aortic wall *in vivo*. This modality uses a blend of radioactive tracers, such as Technetium-99m (^{99m}Tc), iodine-123 (^{123}I), and Indium-111 (^{111}In) emitting gamma rays, and probes specific for cells to create an image.[35, 36] While SPECT imaging may not provide the same spatiotemporal resolution as MRI or PET, it does offer a myriad of other advantages, including being more accessible to bedside imaging of patients, less expensive, and using radionucleotides that decay at a slower rate,

which permits longer time for study.[37, 38] Additionally, SPECT provides a comprehensive 3-dimensional representative image of aneurysm formation.[39]

The use of ^{99m}Tc-cFLFLF based SPECT imaging to target activated PMNs in AAA has important clinical implications. The role of PMNs in AAA formation has been well established as we have previously shown that depletion of circulating neutrophils leads to a decrease in AAA phenotype compared to untreated group in a murine model.[8] Additionally, He *et al* demonstrated that stimulation of formyl peptide receptor (FPR) 1 and FPR2, recruited Mac-1-mediated neutrophils and exacerbated AAA growth, whereas antagonism of these receptors attenuated AAA development.[9] FPR is overexpressed in activated neutrophils and its activation induces release of pro-inflammatory mediators and gene transcription.[16, 17] ^{99m}Tc-cFLFLF is a radiolabeled FPR1 receptor imaging probe that selectively binds to activated PMNs in AAA and allows for noninvasive *in vivo* imaging of inflammation in the aortic wall.[15] The use of this novel imaging tracer has demonstrated efficacy in other disease processes, such as acute intervertebral disk herniation, among others, and holds promise for evaluation of AAA.[12] We observed a sequential increase in fluorescence intensity of c-FLFLF on day 14 compared to day 7 although there was no further enhancement in corresponding neutrophil infiltration. The increase in c-FLFLF intensity is likely due to the increased activation of FPR1 on infiltrating neutrophils that correspond to persistent aortic inflammation. Further studies using our chronic aortic rupture model will help in delineating the c-FLFLF-mediated monitoring of aortic inflammation and progression leading to aortic rupture. Consequently, aortic SPECT imaging with ^{99m}Tc-cFLFLF *in vivo* is a clinically relevant and noninvasive option to track the progression of neutrophil infiltration as well as aortic inflammation and growth of AAA that can potentially predict aortic rupture.

There are a few limitations of this study. The murine AAA model attempts to replicate a chronic disease process that occurs over many years in an acute period, thereby limiting its applicability to human disease. However, our previous studies have demonstrated a remarkable synergy between immunopathology of human AAA tissue and the experimental murine models thereby underlining the importance of the proposed inflammatory signaling pathways.[18, 40, 41] Further studies in large animals i.e. our recently described swine model of AAA as well as murine aortic rupture model will enhance and validate clinical translatability of the c-FLFLF-based SPECT imaging for diagnosing and monitoring the progression of AAA[42–44]. Additionally, as mentioned above, SPECT does not provide the same spatiotemporal resolution as MRI or PET scans. However, an advantage of cFLFLF probe is that it can be coupled with radioisotopes specific for PET, such as Cu-64[14], and future studies can decipher these additional imaging modalities for diagnosing AAA. Finally, although cFLFLF mostly binds activated PMNs, there may be multiple sites of neutrophil mediated inflammation in the body simultaneously, such as infection. The radiolabel could tag all areas of neutrophil activation, including the aneurysmal wall, thereby making differentiation difficult to decipher. However, the spatiotemporal specificity of CT along with SPECT or PET scans does markedly enhance the specificity of aneurysmal inflammation for detection of AAA.

Conclusions

Using an established murine model of AAA, SPECT imaging with tagging of activated neutrophils using ^{99m}Tc-cFLFLF, is a novel noninvasive *in vivo* imaging modality to accurately quantify and characterize inflammation within the aortic wall. This modality shows promise in the early diagnosis of AAA and detection of aortic inflammation by targeting specific activated immune cells i.e. neutrophils.. Future studies will delineate the progression of AAA to aortic rupture to decipher the c-FLFLF-mediated detection and monitoring of progressive aortic inflammation as well as targeting other immune cells implicated in AAA pathophysiology, such as T cells, M1 and M2 macrophages.

Acknowledgement

Funding: This study was supported by grants from American Heart Association Grant-in-Aid (17GRNT33370027) and National Institute of Health (RO1HL081629). We thank Molecular Imaging Core laboratory at University of Virginia for the Albira Trimodal PET/SPECT/CT scanner instrumentation support.

REFERENCES

1. Lederle FA, Johnson GR, Wilson SE, Chute EP, Hye RJ, Makaroun MS, Barone GW, Bandyk D, Moneta GL and Makhoul RG. The aneurysm detection and management study screening program: validation cohort and final results. Aneurysm Detection and Management Veterans Affairs Cooperative Study Investigators. Arch Intern Med. 2000;160:1425–30. [PubMed: 10826454]
2. Lederle FA, Johnson GR, Wilson SE, Littooy FN, Krupski WC, Bandyk D, Acher CW, Chute EP, Hye RJ, Gordon IL, Freischlag J, Averbook AW and Makaroun MS. Yield of repeated screening for abdominal aortic aneurysm after a 4-year interval. Aneurysm Detection and Management Veterans Affairs Cooperative Study Investigators. Arch Intern Med. 2000;160:1117–21. [PubMed: 10789604]
3. Norman PE, Jamrozik K, Lawrence-Brown MM, Le MT, Spencer CA, Tuohy RJ, Parsons RW and Dickinson JA. Population based randomised controlled trial on impact of screening on mortality from abdominal aortic aneurysm. BMJ. 2004;329:1259. [PubMed: 15545293]
4. Cosford PA and Leng GC. Screening for abdominal aortic aneurysm. Cochrane Database Syst Rev. 2007:CD002945.
5. Brewster DC, Cronenwett JL, Hallett JW Jr., Johnston KW, Krupski WC, Matsumura JS, Joint Council of the American Association for Vascular S and Society for Vascular S. Guidelines for the treatment of abdominal aortic aneurysms. Report of a subcommittee of the Joint Council of the American Association for Vascular Surgery and Society for Vascular Surgery. J Vasc Surg. 2003;37:1106–17. [PubMed: 12756363]
6. Shimizu K, Mitchell RN and Libby P. Inflammation and cellular immune responses in abdominal aortic aneurysms. Arterioscler Thromb Vasc Biol. 2006;26:987–94. [PubMed: 16497993]
7. Freestone T, Turner RJ, Coady A, Higman DJ, Greenhalgh RM and Powell JT. Inflammation and matrix metalloproteinases in the enlarging abdominal aortic aneurysm. Arterioscler Thromb Vasc Biol. 1995;15:1145–51. [PubMed: 7627708]
8. Eliason JL, Hannawa KK, Ailawadi G, Sinha I, Ford JW, Deogracias MP, Roelofs KJ, Woodrum DT, Ennis TL, Henke PK, Stanley JC, Thompson RW and Upchurch GR Jr. Neutrophil depletion inhibits experimental abdominal aortic aneurysm formation. Circulation. 2005;112:232–40. [PubMed: 16009808]
9. He L, Fu Y, Deng J, Shen Y, Wang Y, Yu F, Xie N, Chen Z, Hong T, Peng X, Li Q, Zhou J, Han J, Wang Y, Xi J and Kong W. Deficiency of FAM3D (Family With Sequence Similarity 3, Member D), A Novel Chemokine, Attenuates Neutrophil Recruitment and Ameliorates Abdominal Aortic Aneurysm Development. Arterioscler Thromb Vasc Biol. 2018;38:1616–1631. [PubMed: 29853563]

10. Rizas KD, Ippagunta N and Tilson MD 3rd. Immune cells and molecular mediators in the pathogenesis of the abdominal aortic aneurysm. Cardiol Rev. 2009;17:201–10. [PubMed: 19690470]

11. Zhang Y, Xiao L, Chordia MD, Locke LW, Williams MB, Berr SS and Pan D. Neutrophil targeting heterobivalent SPECT imaging probe: cFLFLF-PEG-TKPPR-99mTc. Bioconjug Chem. 2010;21:1788–93. [PubMed: 20843030]

12. Xiao L, Ding M, Zhang Y, Chordia M, Pan D, Shimer A, Shen F, Glover D, Jin L and Li X. A Novel Modality for Functional Imaging in Acute Intervertebral Disk Herniation via Tracking Leukocyte Infiltration. Mol Imaging Biol. 2017;19:703–713. [PubMed: 28050750]

13. Malm BJ and Sadeghi MM. Multi-modality molecular imaging of aortic aneurysms. J Nucl Cardiol. 2017;24:1239–1245. [PubMed: 28447279]

14. Locke LW, Chordia MD, Zhang Y, Kundu B, Kennedy D, Landseadel J, Xiao L, Fairchild KD, Berr SS, Linden J and Pan D. A novel neutrophil-specific PET imaging agent: cFLFLFK-PEG-64Cu. J Nucl Med. 2009;50:790–7. [PubMed: 19372473]

15. Li J, Zhang Y, Chordia MD, Wu H, Shao L and Pan D. Multimodal formyl peptide receptor 1 targeted inflammation imaging probe: cFLFLF-MHI-DOTA. Bioorg Med Chem Lett. 2016;26:1052–1055. [PubMed: 26750259]

16. Schiffmann E, Corcoran BA and Wahl SM. N-formylmethionyl peptides as chemoattractants for leucocytes. Proc Natl Acad Sci U S A. 1975;72:1059–62. [PubMed: 1093163]

17. Lui Y CK, Ming Wang Ji. FPR Ligands In: Kastin AJ, ed. Handbook of Biologically Active Peptides: Elsevier Inc.; 2013: 671–680.

18. Sharma AK, Lu G, Jester A, Johnston WF, Zhao Y, Hajzus VA, Saadatzadeh MR, Su G, Bhamidipati CM, Mehta GS, Kron IL, Laubach VE, Murphy MP, Ailawadi G and Upchurch GR Jr. Experimental abdominal aortic aneurysm formation is mediated by IL-17 and attenuated by mesenchymal stem cell treatment. Circulation. 2012;126:S38–45. [PubMed: 22965992]

19. Charles EJ, Chordia MD, Zhao Y, Zhang Y, Mehaffey JH, Glover DK, Dimastromatteo J, Chancellor WZ, Sharma AK, Kron IL, Pan D and Laubach VE. SPECT imaging of lung ischemia-reperfusion injury using 99mTc-cFLFLF for molecular targeting of formyl peptide receptor 1. Am J Physiol Lung Cell Mol Physiol. 2019.

20. Sakalihasan N, Limet R and Defawe OD. Abdominal aortic aneurysm. Lancet. 2005;365:1577–89. [PubMed: 15866312]

21. Semmens JB, Norman PE, Lawrence-Brown MM and Holman CD. Influence of gender on outcome from ruptured abdominal aortic aneurysm. Br J Surg. 2000;87:191–4. [PubMed: 10671926]

22. Hannawa KK, Eliason JL, Woodrum DT, Pearce CG, Roelofs KJ, Grigoryants V, Eagleton MJ, Henke PK, Wakefield TW, Myers DD, Stanley JC and Upchurch GR Jr. L-selectin-mediated neutrophil recruitment in experimental rodent aneurysm formation. Circulation. 2005;112:241–7. [PubMed: 15998669]

23. Palestro CJ. In vivo leukocyte labeling: the quest continues. J Nucl Med. 2007;48:332–4. [PubMed: 17332607]

24. Ruehm SG, Corot C, Vogt P, Kolb S and Debatin JF. Magnetic resonance imaging of atherosclerotic plaque with ultrasmall superparamagnetic particles of iron oxide in hyperlipidemic rabbits. Circulation. 2001;103:415–22. [PubMed: 11157694]

25. Herborn CU, Vogt FM, Lauenstein TC, Dirsch O, Corot C, Robert P and Ruehm SG. Magnetic resonance imaging of experimental atherosclerotic plaque: comparison of two ultrasmall superparamagnetic particles of iron oxide. J Magn Reson Imaging. 2006;24:388–93. [PubMed: 16791857]

26. Hyafil F, Laissy JP, Mazighi M, Tchetche D, Louedec L, Adle-Biassette H, Chillon S, Henin D, Jacob MP, Letourneur D and Feldman LJ. Ferumoxtran-10-enhanced MRI of the hypercholesterolemic rabbit aorta: relationship between signal loss and macrophage infiltration. Arterioscler Thromb Vasc Biol. 2006;26:176–81. [PubMed: 16269663]

27. Trivedi RA, Mallawarachi C, JM UK-I, Graves MJ, Horsley J, Goddard MJ, Brown A, Wang L, Kirkpatrick PJ, Brown J and Gillard JH. Identifying inflamed carotid plaques using in vivo

USPIO-enhanced MR imaging to label plaque macrophages. Arterioscler Thromb Vasc Biol. 2006;26:1601–6. [PubMed: 16627809]

28. Kooi ME, Cappendijk VC, Cleutjens KB, Kessels AG, Kitslaar PJ, Borgers M, Frederik PM, Daemen MJ and van Engelshoven JM. Accumulation of ultrasmall superparamagnetic particles of iron oxide in human atherosclerotic plaques can be detected by in vivo magnetic resonance imaging. Circulation. 2003;107:2453–8. [PubMed: 12719280]
29. Lin JB, Phillips EH, Riggins TE, Sangha GS, Chakraborty S, Lee JY, Lycke RJ, Hernandez CL, Soepriatna AH, Thorne BR, Yrineo AA and Goergen CJ. Imaging of small animal peripheral artery disease models: recent advancements and translational potential. Int J Mol Sci. 2015;16:11131–77. [PubMed: 25993289]
30. Tang TY, Muller KH, Graves MJ, Li ZY, Walsh SR, Young V, Sadat U, Howarth SP and Gillard JH. Iron oxide particles for atheroma imaging. Arterioscler Thromb Vasc Biol. 2009;29:1001–8. [PubMed: 19229073]
31. Sakalihasan N, Van Damme H, Gomez P, Rigo P, Lapiere CM, Nusgens B and Limet R. Positron emission tomography (PET) evaluation of abdominal aortic aneurysm (AAA). Eur J Vasc Endovasc Surg. 2002;23:431–6. [PubMed: 12027471]
32. English SJ, Piert MR, Diaz JA, Gordon D, Ghosh A, D'Alecy LG, Whitesall SE, Sharma AK, DeRoo EP, Watt T, Su G, Henke PK, Eliason JL, Ailawadi G and Upchurch GR Jr. Increased 18F-FDG uptake is predictive of rupture in a novel rat abdominal aortic aneurysm rupture model. Ann Surg. 2015;261:395–404. [PubMed: 24651130]
33. Courtois A, Nusgens BV, Hustinx R, Namur G, Gomez P, Somja J, Defraigne JO, Delvenne P, Michel JB, Colige AC and Sakalihasan N. 18F-FDG uptake assessed by PET/CT in abdominal aortic aneurysms is associated with cellular and molecular alterations prefacing wall deterioration and rupture. J Nucl Med. 2013;54:1740–7. [PubMed: 24009278]
34. Rafaella P RJ. Neurosonology and noninvasive imaging of the carotid arteries. Handbook of Clinical Neurology. 2016;135:165–191. [PubMed: 27432665]
35. Madsen MT. Recent advances in SPECT imaging. J Nucl Med. 2007;48:661–73. [PubMed: 17401106]
36. Shimizu Y and Kuge Y. Recent Advances in the Development of PET/SPECT Probes for Atherosclerosis Imaging. Nucl Med Mol Imaging. 2016;50:284–291. [PubMed: 27994683]
37. Ramaswamy AK, Hamilton M 2nd, Joshi RV, Kline BP, Li R, Wang P and Goergen CJ. Molecular imaging of experimental abdominal aortic aneurysms. ScientificWorldJournal. 2013;2013:973150.
38. Peremans K, Cornelissen B, Van Den Bossche B, Audenaert K and Van de Wiele C. A review of small animal imaging planar and pinhole spect Gamma camera imaging. Vet Radiol Ultrasound. 2005;46:162–70. [PubMed: 15869162]
39. Brangsch J, Reimann C, Collettini F, Buchert R, Botnar RM and Makowski MR. Molecular Imaging of Abdominal Aortic Aneurysms. Trends Mol Med. 2017;23:150–164. [PubMed: 28110838]
40. Sharma AK, Salmon MD, Lu G, Su G, Pope NH, Smith JR, Weiss ML and Upchurch GR Jr. Mesenchymal Stem Cells Attenuate NADPH Oxidase-Dependent High Mobility Group Box 1 Production and Inhibit Abdominal Aortic Aneurysms. Arterioscler Thromb Vasc Biol. 2016;36:908–18. [PubMed: 26988591]
41. Spinosa M, Lu G, Su G, Bontha SV, Gehrau R, Salmon MD, Smith JR, Weiss ML, Mas VR, Upchurch GR Jr. and Sharma AK. Human mesenchymal stromal cell-derived extracellular vesicles attenuate aortic aneurysm formation and macrophage activation via microRNA-147. FASEB J. 2018:fj201701138RR.
42. Cullen JM, Lu G, Shannon AH, Su G, Sharma A, Salmon M, Fashandi AZ, Spinosa MD, Montgomery WG, Johnston WF, Ailawadi G and Upchurch GR Jr. A novel swine model of abdominal aortic aneurysm. J Vasc Surg. 2019;70:252–260 e2. [PubMed: 30591288]
43. Fashandi AZ, Hawkins RB, Salmon MD, Spinosa MD, Montgomery WG, Cullen JM, Lu G, Su G, Ailawadi G and Upchurch GR Jr. A novel reproducible model of aortic aneurysm rupture. Surgery. 2018;163:397–403. [PubMed: 29195736]

44. Lu G, Su G, Davis JP, Schaheen B, Downs E, Roy RJ, Ailawadi G and Upchurch GR Jr. A novel chronic advanced stage abdominal aortic aneurysm murine model. J Vasc Surg. 2017;66:232–242 e4. [PubMed: 28274752]

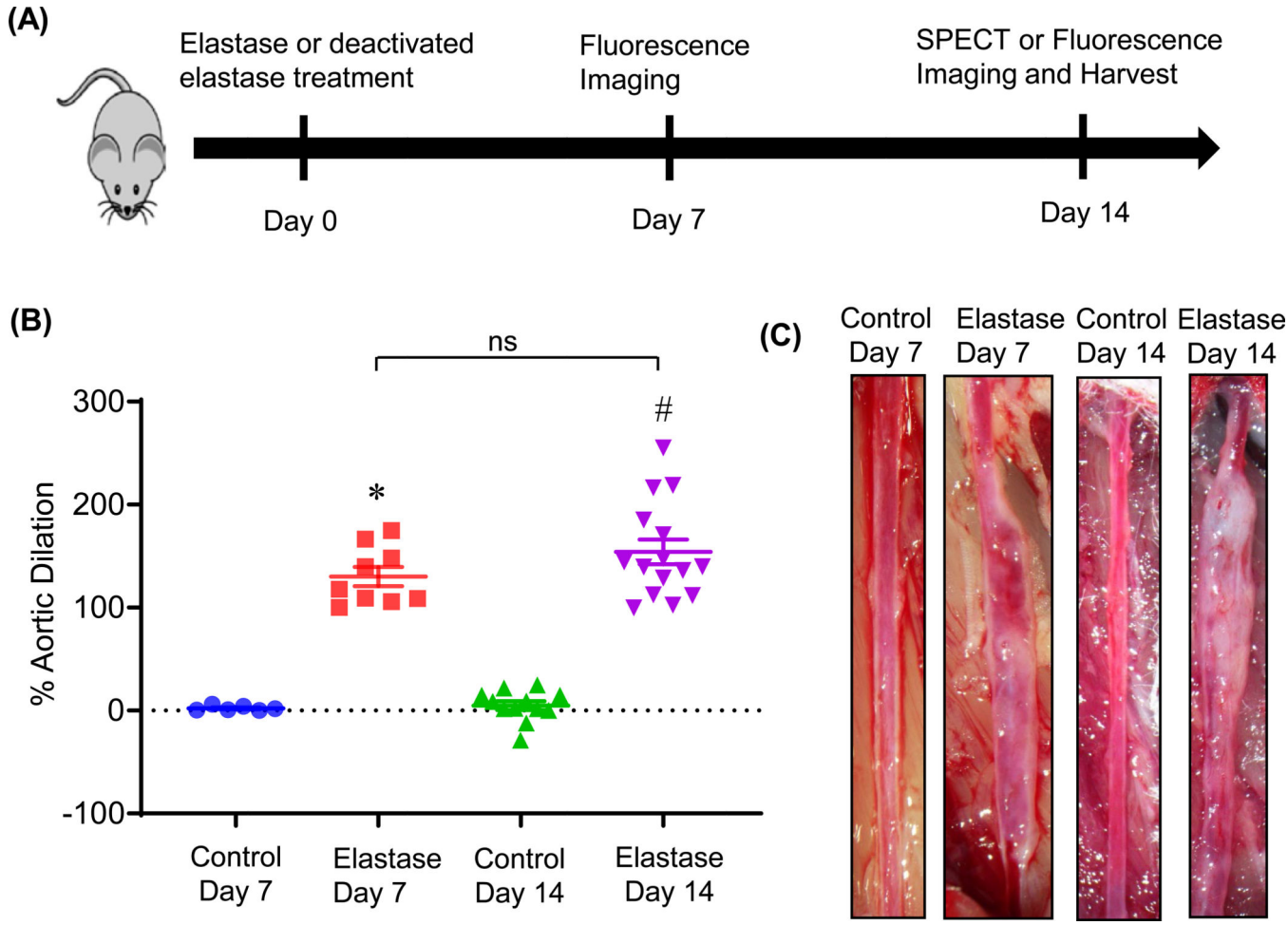

Figure 1. Study design and phenotypic data.

(A) The schematic of the elastase treatment murine model of AAA. Infrarenal mouse aortas were treated with elastase or deactivated elastase (Control). Aortic diameter was measured on days 7 or 14, and tissue was harvested for further analysis. SPECT or fluorescence imaging was performed on days 7 and 14. **(B)** Elastase treated mice demonstrated a significant increase in aortic diameter compared with deactivated elastase treated mice on days 7 and 14, respectively. **(C)** Representative images of aortic phenotype in all groups. Aortic diameter increased in elastase treated groups compared to control groups. $^{*}P<0.0001$ vs. Control Day 7; $^{\#}P<0.0001$ vs. Control Day 14; ns, not significant; n=6–15 mice/group.

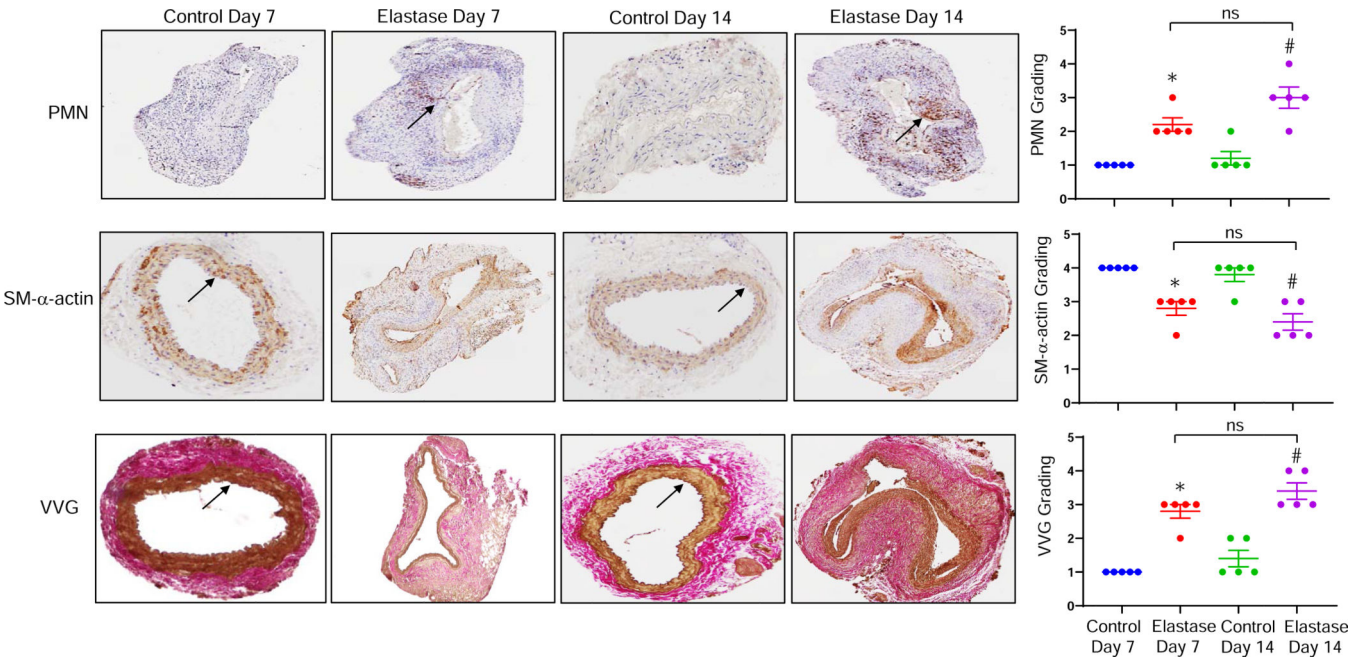

Figure 2. Increased neutrophil infiltration in AAA tissue.

Comparative histology performed on days 7 and 14 indicates that elastase-treated WT mice have a marked increase in neutrophil (PMN) infiltration, a decrease in smooth muscle cell α-actin (SM-αA) expression, as well as increase in elastic fiber disruption (Verhoeff-Van Gieson staining for elastin) compared to deactivated elastase-treated (control) mice, respectively. Quantification of histologic grading indicates a significant increase in neutrophil infiltration, decrease in SM-αA expression and increase in elastic fiber disruption in elastase-treated aortic tissue on days 7 and 14 compared to controls. Arrows indicate areas of immunostaining. $*P<0.005$ vs. Control Day 7; $^{\#}P<0.0005$ vs. Control Day 14; ns, not significant; n=5 mice/group.

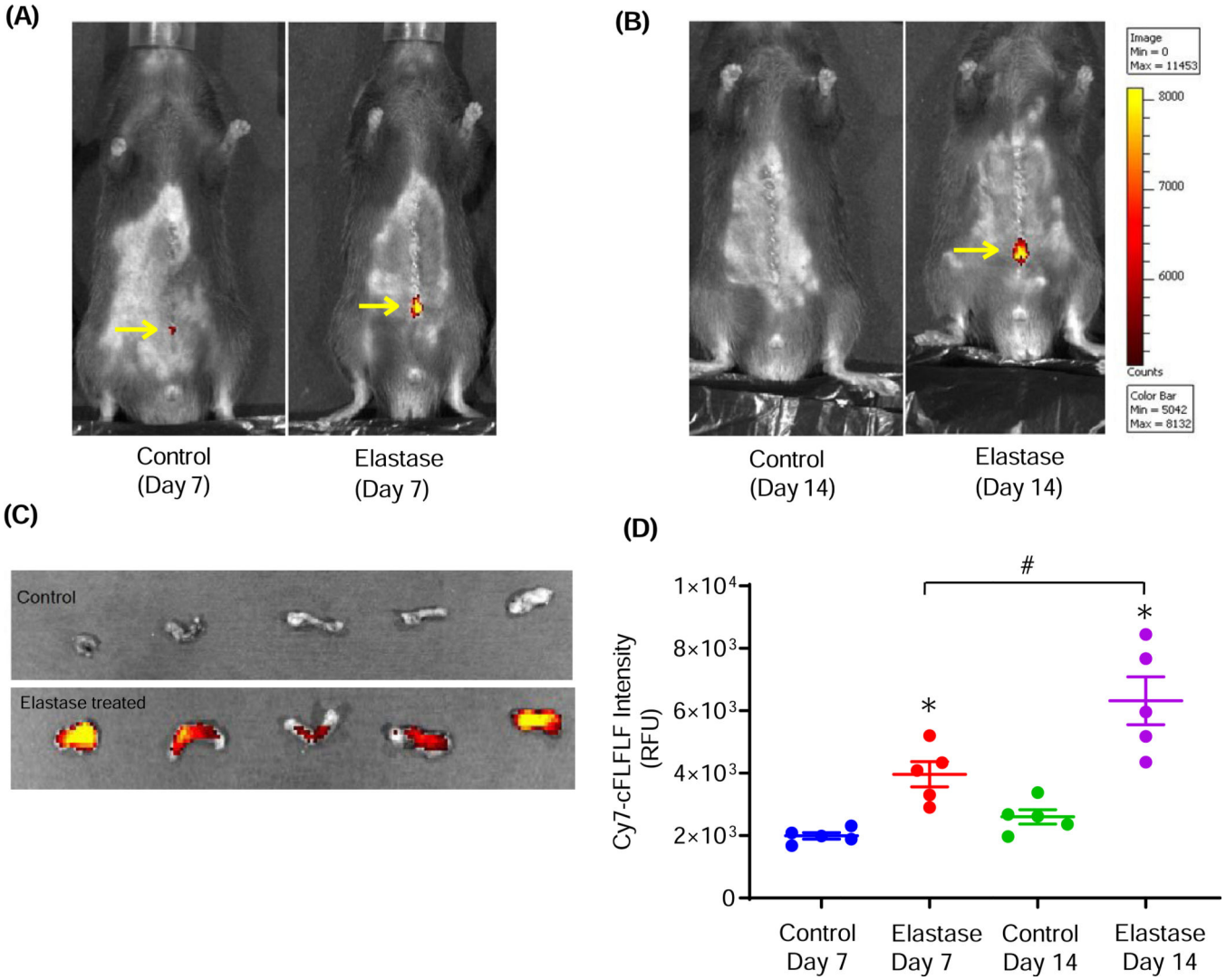

Figure 3. Increased uptake of c-FLFLF in AAA by fluorescence imaging of mice.

Near-infrared fluorescence imaging of c-FLFLF-Cy7 in live (shaved) anesthetized mice demonstrating aortic inflammation (elevated fluorescence) at the site of infrarenal AAA formation (see arrows) compared to controls on days 7 **(A)** and 14 **(B)**. **(C)** Near-infrared fluorescence imaging of c-FLFLF-Cy7 in *ex vivo* aortic tissue demonstrating elevated fluorescence compared to controls on day14. **(D)** Fluorescence intensity (RFU; relative fluorescence units) in *ex vivo* aortic tissue was significantly increased on day 7 as well as on day 14 in elastase-treated mice (AAA) compared to respective controls. **P*<0.05 vs. respective controls; $^{\#}P$<0.05 vs. Elastase Day 7; n=5 mice/group.

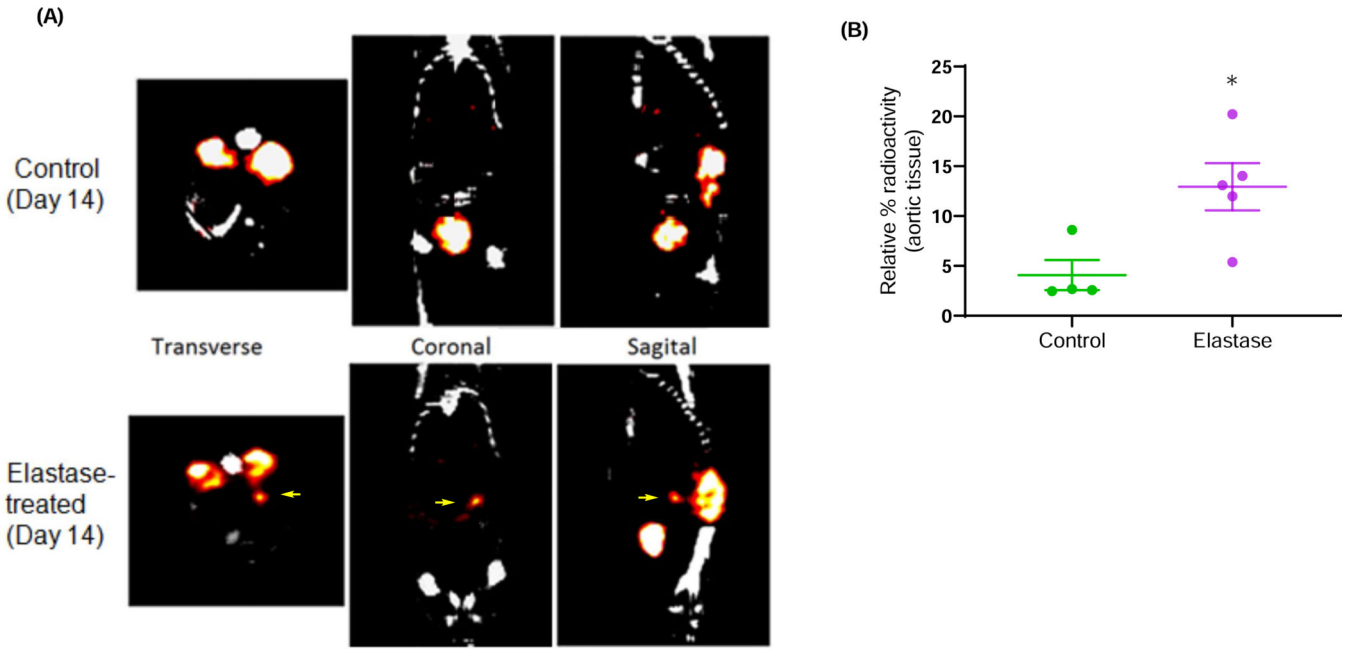

Figure 4. Increased uptake of c-FLFLF in AAA by SPECT/CT imaging of mice.

(A) SPECT/CT imaging using ^{99m}Tc-cFLFLF demonstrated an increase in c-FLFLF uptake (shown by arrows) in elastase-treated mice (AAA) compared to controls on day 14, signifying increased aortic inflammation relative to aneurysms. CT and SPECT scans were utilized to image the animal as it moved along the axis of rotation, allowing for combination of CT and SPECT images using stored offset parameters. **(B)** A significant increase in ^{99m}Tc-cFLFLF radioactivity was observed in harvested aortic tissue from elastase-treated mice compared to controls. *P<0.05 vs. control; n=4–5 mice/group.

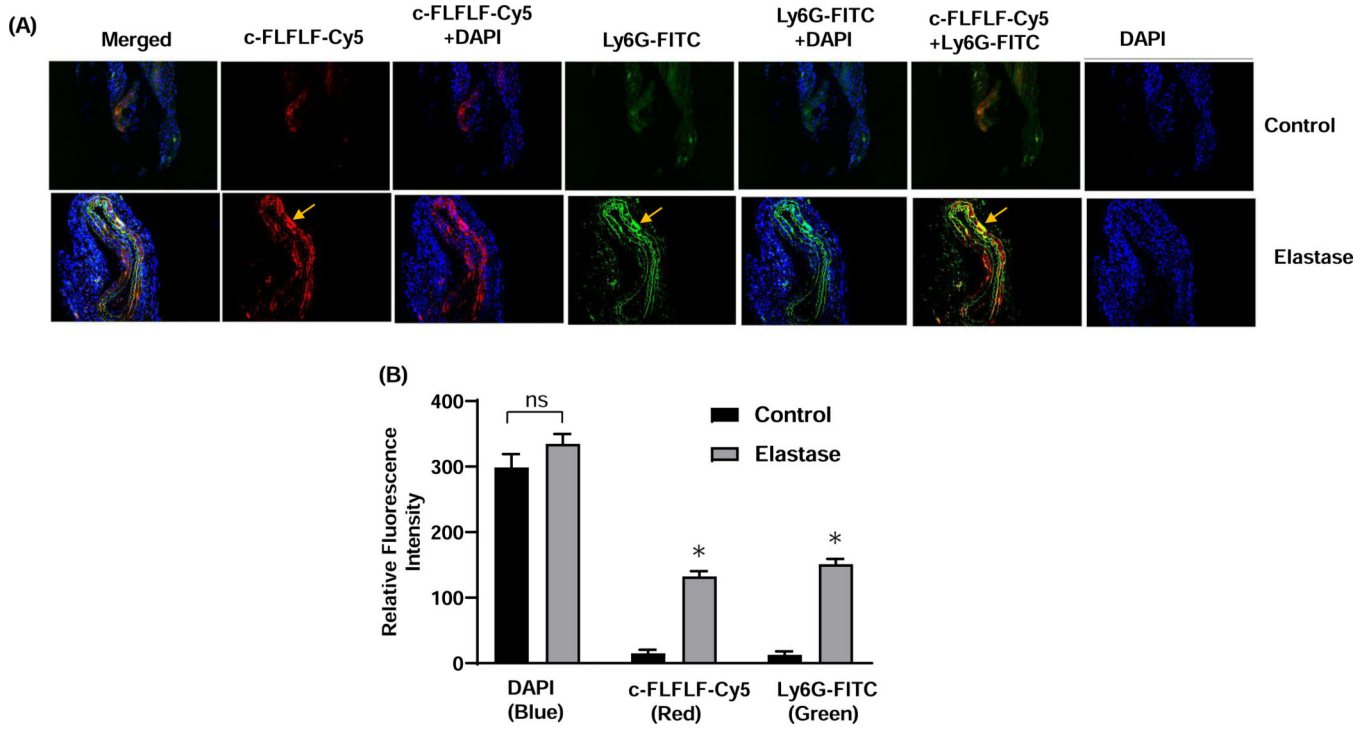

Figure 5. Co-expression of c-FLFLF with PMNs in AAA tissue.

(A) Immunostaining of murine aortic tissue demonstrates increased c-FLFLF-Cy5 (red) expression in elastase-treated WT mice (***bottom panel***) compared to controls (***top panel***) on day 14. A marked increase in neutrophil (Ly6G-FITC; green) expression is also observed in elastase-treated mice compared to control. Moreover, the c-FLFLF expression is co-localized with neutrophils (Ly6G-FITC) indicating the neutrophil-specificity of the c-FLFLF probe. Arrows indicate specific and increased areas of c-FLFLF-Cy5 and Ly6G-FITC expression. **(B)** Quantification of same normalized areas of imaging demonstrates increased fluorescence intensity of c-FLFLF-Cy5 and Ly6G-FITC. ns, not significant; **P*<0.05 vs. respective controls; n=5 mice/group.